J. Fluid Mech. (1994), *vol.* 260, *pp.* 299–314

On the motion of a rigid cylinder in a rotating electrically conducting fluid

By DAVID E. LOPER

Department of Mathematics and Geophysical Fluid Dynamics Institute, Florida State University, Tallahassee, FL 32306-3017, USA

(Received 23 February 1993 and in revised form 31 August 1993)

The flow structures generated and drag experienced by a rigid cylinder moving in an arbitrary direction through a rotating electrically conducting fluid in the presence of an applied magnetic field are investigated, with the aim of understanding better the nature of the small-scale flow in the core of the Earth which may be responsible for maintaining the geomagnetic field through dynamo action. Three cases are considered in the limit of small Rossby and magnetic Reynolds numbers. In the case of very weak rotation, the possible flow structures consist of a thin Hartmann layer and a long wake extending in the direction of the magnetic field, in which Lorentz and viscous forces balance, but only the long wake plays a dynamical role. The dominant drag force is experienced for motion that cuts magnetic lines of force. Motion of the cylinder parallel to its axis induces a much weaker drag, while that in the direction of the magnetic field induces none to dominant order. The cylinder also experiences weak lateral forces due to the Coriolis effect. In the case of weak rotation, the balance in the long wake is now magnetostrophic: between Lorentz and Coriolis forces. The drag is qualitatively identical to that in the first case, but the drag induced by motion parallel to the axis of the cylinder is increased, though still smaller than that for motions cutting magnetic lines of force. In the case of strong rotation, the flow structures consist of a thin Ekman layer and a foreshortened Taylor column extending in the direction of the rotation axis. In this column, the force balance is again magnetostrophic. Again only the large-scale structure plays a dynamical role. Motion of the cylinder perpendicular to its axis induces a larger drag than does motion parallel to its axis. The cylinder also experiences large lateral Coriolis forces.

1. Introduction

This paper is motivated by a desire to understand better the small-scale flow within the Earth's core which may be responsible for driving the dynamo which sustains the Earth's magnetic field. The most likely power source for the geodynamo is compositional convection driven by the excess of light material released by the gradual solidification of the inner core as the Earth cools over geologic time (Braginsky 1963; Lowes 1984). Laboratory experiments (Tait & Jaupart 1989, 1992; Chen & Chen 1991) suggest that this material is released in the form of compositionally buoyant plumes and blobs which rise through the outer core.

These rising buoyant parcels are acted on by three non-coplanar forces, due to gravity, rotation and the ambient magnetic field. The direction and rate of rise of parcels under such circumstances is unknown. The problem of determining rise velocity is very difficult for a fluid parcel, since the parcel will in general be deformed by the flow, yielding a free-boundary problem. As a preliminary to solving this problem, we

shall consider the simpler, but still challenging, problem of determining the drag on a rigid body of known shape. This restriction is not as severe as one would expect, since the rate of distortion of a buoyant parcel is much slower than the adjustment of the flow in response to a given buoyancy distribution. Therefore, studies of the rise of rigid parcels is expected to give results that are similar to the more difficult problem of the rise of buoyant fluid parcels.

In the present paper we shall consider the motion of a rigid circular cylinder; a rigid sphere will be considered in a later paper. The motivation for considering cylindrical shapes is provided by a simple illustrative experiment involving the cooling of ammonium chloride in which buoyant material rises from the bottom boundary in the form of cylinders (see Eltayeb & Loper 1991, figure 1). It may be argued that turbulence within the core would destroy these cylindrical shapes, but the scaling argument presented in Moffatt & Loper (1993, §6) suggests that they might indeed retain their identity and geometry. Therefore the results of the present analysis might have direct application to buoyancy-driven flow within the core.

The cylinder is assumed to be in steady translational motion in an arbitrary direction through a homogeneous rotating fluid of infinite extent in the presence of a uniform magnetic field. The orientations of the rotation and magnetic-field vectors are arbitrary. We shall assume that the velocity of the cylinder is known and calculate the drag acting on it.

Calculation of the flow field produced by, and drag experienced by, a translating cylinder in a non-rotating, non-conducting fluid is classic problem of fluid dynamics. For transverse motion (i.e. perpendicular to the cylinder axis) the Oseen approximation permits a uniformly valid solution, while no steady solution exists for the case of motion parallel to the axis. This singular behaviour is removed by the presence of the rotation and magnetic field. The rotational and hydromagnetic effects make the fluid medium anisotropic, and the effect of the cylinder is channelled into narrow structures, rather than affecting all the surrounding fluid. A natural consequence of this anisotropy is that the drag force is a general linear function of the prescribed velocity. In the following sections we shall determine the tensor of drag coefficients (referred to as the drag tensor) which relates these two vectors.

The effects of rotational and hydromagnetic forces are measured by two dimensionless parameters (see (2.6)) measuring the relative strengths of Coriolis, Lorentz and viscous forces. These forces combine to give the well-known Ekman–Hartmann boundary layers, plus less familiar large-scale structures. In the case in which Lorentz forces dominate Coriolis ones in the boundary-layer structure, the large-scale structure is elongated in the direction of the magnetic field, while in the opposite case, it is elongated in the direction of the rotation vector. The effect of these elongations is to weaken the dominant force, making a balance with the weaker force possible. Each of these elongated structures can be thought of as a magnetostropic balance. In the extreme case of very weak rotation the large-scale balance is between Lorentz and viscous forces, while in the case of very strong rotation, it is between Coriolis and viscous forces. This latter case yields the familiar Taylor column. These balances are summarized in table 1. We shall assume that the Hartmann number is large, so that the case of very strong rotation is not considered in the present paper. The strength of the magnetic field within the Earth's core is very poorly known, as the toroidal part is unobserved. However, it is generally believed that the toroidal field is sufficiently large that the case of weak rotation pertains to the core.

There have been very few studies of cylinders in hydromagnetic flow. A flow configuration in which there would be no distortion of the cylinder if it were fluid has

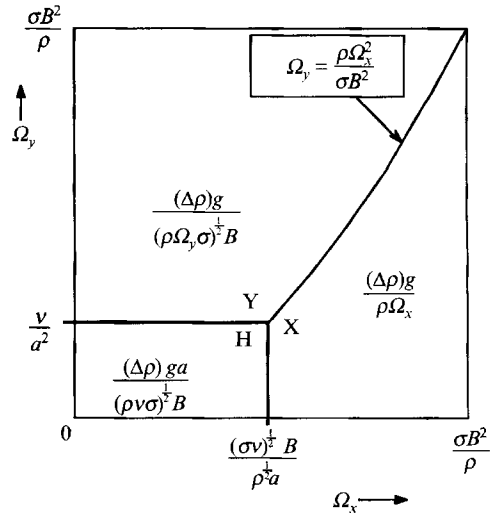

FIGURE 1. Dimensional rise speeds for the three flow regimes within the parameter box Ω_x, $\Omega_y < \sigma B^2/\rho$. Those for regimes H and Y are calculated, while that for regime X is conjectured. The rise speeds agree at the common boundaries.

Short-scale	Large-scale	Direction of elongation
Very-weak rotation ($N \ll 1/M$, $1 \ll M$, $1 \ll E$)		
$L = V$	$L = V$	Along B
Weak rotation ($1/M \ll N \ll 1$, $1 \ll M$, $E \ll 1$)		
$L = V$	$L = C$	Along B
Strong rotation ($1 \ll N$, $1 \ll M$, $E \ll 1$)		
$C = V$	$L = C$	Along Ω
Very strong rotation ($1 \ll N$, $M \ll 1$, $E \ll 1$)		
$C = V$	$C = V$	Along Ω

TABLE 1. Force balances: L = Lorentz, C = Coriolis, V = Viscous. The parameters M and $N = N_y$ are from (2.6), while $E = (MN)^{-2}$ is the Ekman number

been recently studied by Loper & Moffatt (1993). This consists of a vertical cylinder of buoyant fluid rising parallel to its axis through a fluid rotating about that same axis and permeated by a large-scale transverse magnetic field. Such a flow configuration might exist in the polar regions of the core. This configuration is singular in that the Coriolis force plays no role since all motion is parallel to the axis of rotation. They found that the rate of rise of the buoyant cylinder of fluid is exceptionally rapid in this case, being of the order of $(\Delta\rho)\,ga/B(\rho\sigma\nu)^{\frac{1}{2}}$, where $\Delta\rho$ is the density deficit of the buoyant cylinder and a is a measure of the lateral extent of the cylinder (in the direction of the applied magnetic field of strength B); the remaining notation is standard. This rate of rise is larger than that expected by simple scaling arguments by a factor $M = aB(\sigma/\rho\nu)^{\frac{1}{2}}$.

The analysis of Loper & Moffatt has been generalized by Ruan & Loper (1993). In their study the cylinder was again assumed to move parallel to its axis but the orientations of the rotation and magnetic-field vectors were allowed to be arbitrary. In this circumstance, the cylinder must be assumed rigid, since distortion by the flow would otherwise result. It was found that the rise law of Loper & Moffatt is valid provided the rate of rotation in the direction perpendicular to the applied magnetic

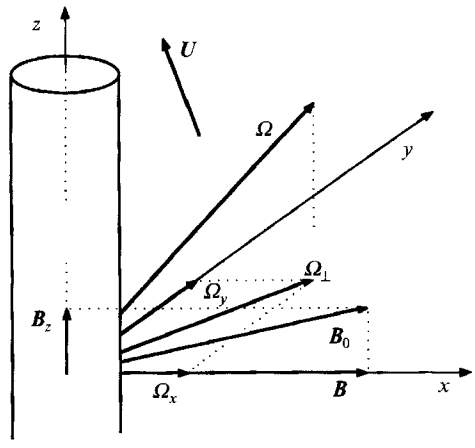

FIGURE 2. Geometric orientation of the cylinder, rotation axis, applied magnetic field, prescribed velocity vector and the Cartesian frame of reference.

field (Ω_y) is less than ν/a^2 and the rate of rotation in the direction of the applied magnetic field (Ω_x) is less than $(\sigma\nu)^{\frac{1}{2}}B/\rho^{\frac{1}{2}}a$. If the first of these conditions is not satisfied, the rate of rise of the cylinder parallel to its axis is of the order of $(\Delta\rho)\,g/B(\rho\sigma\Omega_y)^{\frac{1}{2}}$. This rise law is valid provided $\Omega_y < \sigma B^2/\rho$ and $\Omega_y < \rho\Omega_x^2/\sigma B^2$. If the second condition is not satisfied, the rate of rise has been conjectured to be of the order of $(\Delta\rho)\,g/\rho\Omega_x$. Note that each of these rise laws is independent of the size of the cylinder, and each is much larger than that expected from simple scaling arguments. These rise laws are summarized in figure 1, taken from Ruan & Loper. Note that if Ω_x, Ω_y and B tend to zero such that figure 1 remains valid, the rise speeds all tend to infinity, as expected, since the corresponding non-rotating, non-magnetic problem has no solution.

These previous results hold for a cylinder of buoyant material moving parallel to its axis, and it has been found that the rise speed is anomalously large, in the strong magnetic-field limit, for any orientation of rotation and magnetic field. We now wish to consider the transverse motion of a cylinder, and determine whether this anomaly persists. The major goal of the present study is to determine the drag on the cylinder and to investigate the structure and dynamics of the associated flow structures.

The problem is formulated in §2, and the possible flow structures that may occur are discussed in §3. Also, an expression for the drag force is developed. The three cases of very weak rotation, weak rotation and strong rotation are considered in §§4, 5, and 6. Finally the results are summarized in §7.

2. Formulation

We consider the steady translational motion of a rigid circular cylinder of radius a through a homogeneous rotating fluid of infinite extent in the presence of a uniform magnetic field. The applied magnetic field is assumed to have an arbitrary orientation. The relative orientations of the cylinder, the associated velocity, rotation and magnetic-field vectors and the coordinate system are depicted in figure 2.

The flow is assumed to be steady when viewed from a coordinate frame moving with the cylinder. In this frame the governing equations are given by the set (2.1) of Ruan & Loper (1993). If we let the z-axis of a Cartesian coordinate system coincide with the axis of the cylinder, and the x-axis lie in the plane defined by that axis and the direction

of the applied magnetic field, we may write the velocity $\boldsymbol{u}$, magnetic field $\boldsymbol{B}$ and pressure p as

$$\left.\begin{aligned} \boldsymbol{u} &= -\boldsymbol{U}+|\boldsymbol{U}|\left[\frac{\partial\psi^*}{\partial y^*}\hat{\boldsymbol{x}}-\frac{\partial\psi^*}{\partial x^*}\hat{\boldsymbol{y}}+w^*\hat{\boldsymbol{z}}\right], \\ \boldsymbol{B} &= B\hat{\boldsymbol{x}}+B_z\hat{\boldsymbol{z}}+|\boldsymbol{U}|\,a\mu\sigma B\left[\frac{\partial\phi^*}{\partial y^*}\hat{\boldsymbol{x}}-\frac{\partial\phi^*}{\partial x^*}\hat{\boldsymbol{y}}+c^*\hat{\boldsymbol{z}}\right], \\ p &= p_0+\rho\boldsymbol{r}\cdot\boldsymbol{g}+\tfrac{1}{2}\rho\boldsymbol{\Omega}\times\boldsymbol{r}_c\cdot\boldsymbol{\Omega}\times\boldsymbol{r}_c+|\boldsymbol{U}|\,a\sigma B^2p^*, \quad \text{and} \quad \boldsymbol{\nabla}=\boldsymbol{\nabla}^*/a. \end{aligned}\right\} \tag{2.1}$$

The case in which $\boldsymbol{U}$ is solely in the z-direction has been considered by Ruan & Loper (1993), and that analysis will provide some guidance in what follows. ψ^* is the fluid stream function and ϕ^* is the magnetic-field stream function for the plane perpendicular to the axis of the cylinder. Note that, since the electric current may be expressed as $\boldsymbol{j}=\mu^{-1}\boldsymbol{\nabla}\times\boldsymbol{b}$, the function c^* serves as a stream function for the electric current flowing in the (x,y)-plane and the function $-\nabla^{*2}\phi^*$ equals the electric current flowing in the z-direction. With the chosen geometry, we have that $\partial/\partial z=0$.

Dropping the asterisks, the dimensionless governing equations for $1<x^2+y^2$ are

$$R_0N_y^2\left[\left(\frac{\partial\psi}{\partial y}-u_x\right)\frac{\partial w}{\partial x}-\left(\frac{\partial\psi}{\partial x}+u_y\right)\frac{\partial w}{\partial y}\right]-N_x^2\frac{\partial\psi}{\partial x}-N_y^2\frac{\partial\psi}{\partial y}$$
$$=\frac{\partial c}{\partial x}+R_m\left[\frac{\partial\phi}{\partial y}\frac{\partial c}{\partial x}-\frac{\partial\phi}{\partial x}\frac{\partial c}{\partial y}\right]+\frac{1}{M^2}\nabla^2w, \tag{2.2}$$

$$0=\frac{\partial w}{\partial x}+\nabla^2c, \tag{2.3}$$

$$R_0N_y^2\left[\left(\frac{\partial\psi}{\partial y}-u_x\right)\nabla^2\frac{\partial\psi}{\partial x}-\left(\frac{\partial\psi}{\partial x}+u_y\right)\nabla^2\frac{\partial\psi}{\partial y}\right]+N_x^2\frac{\partial w}{\partial x}+N_y^2\frac{\partial w}{\partial y}$$
$$=-\frac{\partial^2\psi}{\partial x^2}+R_m\left[\frac{\partial\phi}{\partial x}\frac{\partial^2\psi}{\partial x\,\partial y}-\frac{\partial\phi}{\partial y}\frac{\partial^2\psi}{\partial x^2}\right]+\frac{1}{M^2}\nabla^4\psi, \tag{2.4}$$

$$0=\frac{\partial\psi}{\partial x}+\nabla^2\phi; \tag{2.5}$$

where
$$M=aB(\sigma/\rho\nu)^{\frac{1}{2}}, \quad N_i^2=2\rho(\boldsymbol{\Omega}\cdot\hat{\boldsymbol{\imath}})/\sigma B^2 \tag{2.6}$$

and $u_i=(\boldsymbol{U}\cdot\hat{\boldsymbol{\imath}})/|\boldsymbol{U}|$ for $i=x$, y and z, and

$$R_0=(\boldsymbol{U}\cdot\hat{\boldsymbol{z}})/2a(\boldsymbol{\Omega}\cdot\hat{\boldsymbol{y}}), \quad \text{and} \quad R_m=(\boldsymbol{U}\cdot\hat{\boldsymbol{z}})\,a\mu\sigma.$$

The Hartmann number, M, measures the relative strength of the Lorentz and viscous forces, while the magnetic interaction parameters, N_i, measure the relative strengths of the Coriolis and Lorentz forces. (Note that $N^{-2}=EM^2$ where E is the Ekman number; also N^2 is an inverse Elsasser number.) R_0 is the Rossby number and R_m is the magnetic Reynolds number.

We shall assume that $1\ll M$, so that the Lorentz forces are typically much stronger than viscous forces. This assumption rules out the case of very strong rotation, listed in table 1. Also, we shall assume that R_0 and R_m are sufficiently small that the nonlinear inertia terms and nonlinear Lorentz terms appearing in (2.3) and (2.5) are negligibly small. Following the line of argument presented in Ruan & Loper (1993) it may be

verified *a posteriori* that the linearization is valid provided that $R_0 N_y^4 M^3 \ll 1$ and $R_m N_y^2 M \ll 1$ in the case of very weak rotation (having $N_y M \ll 1 \ll M$), $R_0 N_y \ll 1$ and $R_m N_y \ll 1$ in the case of weak rotation (having $1/M \ll N_y \ll 1 \ll M$) or in the case of strong rotation (having $1 \ll N_y$ and $1 \ll M$). These conditions are weaker than the usual conditions that R_0 and R_m be smaller than unity in the case of very weak or weak rotation, but are more severe in the case of strong rotation. Using the parameter estimates of Moffatt & Loper (1993) it may be verified that these conditions are easily satisfied within the core, except that the condition on the magnetic Reynolds number is not strictly satisfied for a large cylinder ($a > 10$ km) if $N_y \geqslant 1$. However, as noted in Moffatt & Loper, the low-R_m approximation generally gives a good qualitative description even when R_m is moderately large.

The above equations hold within the fluid exterior to the cylinder. Within the cylinder the velocity is zero as measured from our moving coordinate system and the magnetic diffusion equation for $x^2+y^2 < 1$ is simply

$$\nabla^2\phi - u_y = \nabla^2 c = 0. \tag{2.7), (2.8}$$

The factor $-u_y$ in the equation governing ϕ for $x^2+y^2 < 1$ represents the applied electric field.

These equations are to be solved subject to the following conditions.

$$\text{As } x^2+y^2 \to \infty: \qquad \psi \to 0, \quad w \to 0, \quad \text{etc.} \tag{2.9}$$

$$\left.\begin{aligned} &\text{At } x^2+y^2 = 1: \\ &\psi = u_x \sin(\theta) - u_y \cos(\theta), \quad \partial\psi/\partial r = u_x \sin(\theta) - u_y \cos(\theta), \\ &w = u_z, \quad \text{and} \quad c, \phi, q\partial c/\partial r \text{ and } \partial\phi/\partial r \text{ are continuous,} \end{aligned}\right\} \tag{2.10}$$

where $u_x^2+u_y^2+u_z^2 = 1$ and

$$q = \begin{cases} 1 & \text{for} \quad 1 < x^2+y^2 \\ \sigma_c/\sigma & \text{for} \quad x^2+y^2 < 1. \end{cases}$$

Here r and θ are the usual cylindrical coordinates: $x = r\cos(\theta)$, $y = r\sin(\theta)$, and σ and σ_c represent the electrical conductivity of the fluid and the rigid cylinder.

The (dimensional) drag force (per unit length) is given by an integral over the surface of the cylinder at $r = a$ of the stress plus an integral over the interior of the cylinder of electromagnetic body force:

$$\boldsymbol{D} = \int_{-\pi}^{\pi} \hat{\boldsymbol{r}} \cdot \boldsymbol{\tau} a \, \mathrm{d}\theta + \int_{-\pi}^{\pi} \int_0^a \frac{1}{\mu} (\nabla \times \boldsymbol{B}) \times \boldsymbol{B} r \, \mathrm{d}r \, \mathrm{d}\theta.$$

Following and generalizing the development in Ruan & Loper (1993), the drag may be expressed in component form as

$$\begin{aligned} \frac{\boldsymbol{D}}{\sigma B^2 |\boldsymbol{U}| a^2} = {} & \pi(N_y^2 \hat{\boldsymbol{x}} - N_x^2 \hat{\boldsymbol{y}}) u_z - \pi N_z^2 (u_y \hat{\boldsymbol{x}} - u_x \hat{\boldsymbol{y}}) + \hat{\boldsymbol{z}} \int_{-\pi}^{\pi} (c)_{r=1} \cos(\theta) \, \mathrm{d}\theta \\ & + \frac{1}{M^2} \int_{-\pi}^{\pi} \left[\hat{\boldsymbol{y}} \left(\frac{\partial^3 \psi}{\partial r^3} \right)_{r=1} + \hat{\boldsymbol{\theta}} \left(\frac{\partial^3 \psi}{\partial r^3} - \frac{\partial^2 \psi}{\partial r^2} \right)_{r=1} + \hat{\boldsymbol{z}} \left(\frac{\partial w}{\partial r} \right)_{r=1} \right] \mathrm{d}\theta. \end{aligned} \tag{2.11}$$

The drag vector is a linear function of the velocity vector; the coefficients of this relationship form a tensor. In §§4–6, we shall find the drag tensor for three parameter ranges. We shall find the drag tensor to be non-symmetric and with components being typically of differing orders of magnitude.

3. Flow structures

The system under investigation has a single scalar operator which in the present case may be expressed in dimensionless form as

$$\left[\left(N_x^2\frac{\partial}{\partial x}+N_y^2\frac{\partial}{\partial y}\right)^2\nabla^2+\left(\frac{\partial^2}{\partial x^2}-\frac{1}{M^2}\nabla^4\right)^2\right] \tag{3.1}$$

with $\nabla^2=\partial^2/\partial x^2+\partial^2/\partial y^2$. This is an eighth-order operator; we anticipate it will yield four decaying modes in a given direction. Note that the components of rotation and magnetic field parallel to the axis of the cylinder play no role in determining the flow structures. There are three regimes of flow as described in the following paragraphs.

For very weak rotation ($N_y \ll 1/M$ and $N_x \ll 1/M^{\frac{1}{2}}$) we have the usual Hartmann layer, plus a very long Braginsky–Hasimoto (BH) structure extending in the direction of the applied magnetic field in which Lorentz and viscous forces are important. The BH balance has been studied by Braginsky (1960), Hasimoto (1960) and Loper & Moffatt (1993). In the BH balance, a weak axial viscous force, produced by velocity gradients in the lateral direction (i.e. perpendicular to the plane of the cylinder and magnetic field), balances an axial Lorentz force which is weakened by the elongation of structure in the direction of the field. The Hartmann layer and the BH structure each yield two modes. This parameter regime is studied in §4.

For weak rotation ($1/M \ll N_y \ll 1$ and $N_x^2 \ll N_y$) the Hartmann structure is unchanged, but the BH structure is replaced by the shorter Ruan structure (Ruan 1993; Loper & Ruan 1993). In this new structure Lorentz and Coriolis forces balance. Since the Coriolis force is stronger than the viscous force, the Lorentz force need not be weakened so dramatically as in the previous case. Consequently the Ruan structure extends a shorter distance $1/N_y$ in the direction of the applied magnetic field. This is a magnetostrophic balance. Again the Ruan structure and the Hartmann layer each yield two modes. This parameter regime is studied in §5.

For strong rotation ($1 \ll N_y$), the large-scale structure extends in the direction of the rotation vector, rather than the magnetic field. In this case, it is convenient to introduce new coordinates having their axes aligned with rotation rather than the magnetic field. Let

$$x=\frac{\Omega_y\xi+\Omega_x\eta}{(\Omega_x^2+\Omega_y^2)^{\frac{1}{2}}}=\xi\cos(\gamma)+\eta\sin(\gamma) \tag{3.2}$$

and

$$y=\frac{-\Omega_x\xi+\Omega_y\eta}{(\Omega_x^2+\Omega_y^2)^{\frac{1}{2}}}=-\xi\sin(\gamma)+\eta\cos(\gamma), \tag{3.3}$$

where $N_x^2=N^2\sin(\gamma)$ and $N_y^2=N^2\cos(\gamma)$ and γ is the angle between the projection of the rotation vector in the (x,y)-plane and the y-axis (see figure 3). The scalar operator (3.1) becomes

$$\left\{\frac{\partial^2}{\partial\eta^2}\nabla^2+\left[\frac{1}{N^2}\left(\cos(\gamma)\frac{\partial}{\partial\xi}+\sin(\gamma)\frac{\partial}{\partial\eta}\right)^2-E\nabla^4\right]^2\right\}, \tag{3.4}$$

where now $\nabla^2=\partial^2/\partial\xi^2+\partial^2/\partial\eta^2$ and $E=(MN)^{-2}$ is the Ekman number.

In the parameter range $1 \ll N$, operator (3.4) yields the familiar Ekman layer to dominant order, plus an elongated structure, of extent $N^2/\cos^2(\gamma)$ in the η-direction, i.e. in the direction of the rotation vector. In this structure, the Coriolis force is sufficiently weakened by the elongation that it balances the Lorentz force. This new structure is similar to a Taylor column, except that the Lorentz force, rather than the

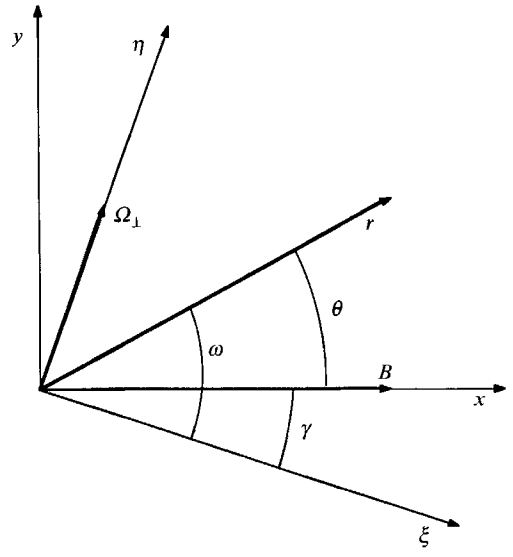

FIGURE 3. The relative orientation of the x, y, z and ξ, η, z coordinate systems.

Size of N_y	Ekman–Hartmann	Large-scale	
$0 < N_y < 1/M$	$\partial/\partial x = \partial/\partial y = M$	$\partial/\partial x = 1/M$	$\partial/\partial y = 1$
$1/M < N_y < 1$	$\partial/\partial x = \partial/\partial y = M$	$\partial/\partial x = N_y$	$\partial/\partial y = 1$
$1 < N_y$	$\partial/\partial x = \partial/\partial y = E^{-\frac{1}{2}}$	$\partial/\partial \xi = 1$	$\partial/\partial \eta = 1/N_y^2$

TABLE 2. Scales of flow structures

viscous force, balances the Coriolis one; this is a magnetostrophic balance. Since the Lorentz force is stronger than the viscous force, the Taylor-like column is now foreshortened compared with the classical form. If the angle between the rotation vector and the y-axis is so close to $\frac{1}{2}\pi$ that $M \ll \tan(\gamma)$ (i.e. if $M^{\frac{1}{2}}N_y \ll N_x$), the Lorentz force becomes weaker than the lateral viscous force and now the balance is between Coriolis and viscous forces; this is the usual Taylor column. The fourth mode comes from a Laplacian. The parameter regime $1 \ll N$ and $\tan(\gamma) \ll M$ is studied in §6.

The scales of structures resulting from the single scalar operator are summarized in table 2, on the assumption that the Coriolis force perpendicular to the magnetic field is dominant and that parallel to the magnetic field is negligible.

4. Solution for very weak rotation: $N_y \ll 1/M$ and $N_x \ll 1/M^{\frac{1}{2}}$

In this parameter range Coriolis forces are unimportant to dominant order and the primary balances are between Lorentz and viscous forces. These forces balance on two disparate lengthscales. There is a short-range Hartmann balance having $\partial/\partial r = O(M)$ and a long-range BH balance (Braginsky 1960; Hasimoto 1960) having $\partial/\partial x = O(1/M)$. Each of these balances produces two modes. In deriving the solutions, it is useful to note the following symmetries. The part of ψ driven by u_x is even in x and odd in y; the part of ψ driven by u_y is odd in x and even in y; w is even in both x and y; c is odd in x and even in y. Note also that on the cylinder $\cos(\theta)$ is odd in x and even in y, while $\sin(\theta)$ is even in x an odd in y.

The governing equations are (2.2)–(2.4) with the terms proportional to R_0, R_m and N_i^2 being omitted and Laplacians reduced to $\partial^2/\partial y^2$. These are to be solved subject to conditions (2.9) and (2.10). With Coriolis effects ignored, the modes are uncoupled in both the Hartmann and BH structures, with one mode for ψ and another for w and c.

The BH modes may be found by contracting the x-axis by a factor M. This collapses the cylinder into a thin ribbon of effectively zero extent on the (y,z)-plane. The governing equations then may be solved by Fourier transform in y. The solutions which obey the symmetry conditions are

$$\psi_{\mathrm{BH}} = \int_0^\infty [u_x \bar{\psi}_x(k) \sin(ky) + \operatorname{sgn}(x)\, u_y \bar{\psi}_y(k) \cos(ky)] \exp(-k^2|x|/M)\, \mathrm{d}k, \quad (4.1)$$

$$w_{\mathrm{BH}} = u_z \int_0^\infty \bar{w}(k) \cos(ky) \exp(-k^2|x|/M)\, \mathrm{d}k, \quad (4.2)$$

and

$$c_{\mathrm{BH}} = -\frac{\operatorname{sgn}(x)\, u_z}{M} \int_0^\infty \bar{w}(k) \cos(ky) \exp(-k^2|x|/M)\, \mathrm{d}k, \quad (4.3)$$

where $\bar{\psi}_x(k)$, $\bar{\psi}_y(k)$ and $\bar{w}(k)$ are functions to be determined by satisfaction of the boundary conditions.

At $x^2+y^2=1$, the combined solutions must satisfy conditions (2.10). Scaling arguments (not presented) show that the conditions on ψ and w are satisfied by the BH modes to dominant order, which require that

$$\int_0^\infty \bar{\psi}_x(k) \sin(ky)\, \mathrm{d}k = \sin(\theta) = y, \quad (4.4)$$

$$\operatorname{sgn}(x) \int_0^\infty \bar{\psi}_y(k) \cos(ky)\, \mathrm{d}k = -\cos(\theta) = -\operatorname{sgn}(x)(1-y^2)^{\frac{1}{2}}, \quad (4.5)$$

and

$$\int_0^\infty \bar{w}(k) \cos(ky)\, \mathrm{d}k = 1. \quad (4.6)$$

These conditions are valid only for $|y|<1$. For $1<|y|$, symmetry requires that

$$\int_0^\infty \bar{\psi}_y(k) \cos(ky)\, \mathrm{d}k = 0. \quad (4.7)$$

The symmetry conditions on $\bar{\psi}_x(k)$ and $\bar{w}(k)$ are automatically satisfied.

Equations (4.5) and (4.7) form a set of dual integral equations for $\bar{\psi}_y(k)$. It may be verified by use of Gradshteyn & Ryzhik (1980, eqns. 6.671.2 (p. 730), 6.693.1 and 6.693.2 (p. 743)) that the solutions of (4.4)–(4.7) are

$$\bar{\psi}_x(k) = J_1(k)/k, \quad \bar{\psi}_y(k) = -J_1(k)/k, \quad \bar{w}(k) = J_1(k), \quad (4.8)$$

where J_1 is a Bessel function of order 1.

The Hartmann modes are weakly driven since the non-homogeneous boundary conditions on ψ and w given by (2.10) are entirely satisfied by the BH mode; only the condition on $\partial\psi/\partial r$ is not satisfied. Consequently the Hartmann mode for w and c has zero amplitude to dominant order, while that for the stream function has an amplitude of order $1/M$:

$$\psi_{\mathrm{H}} = \frac{\operatorname{sgn}(x)\, u_y}{M[\cos(\theta)]^2} \exp[-|\cos(\theta)|\, M(r-1)], \quad w_{\mathrm{H}} = c_{\mathrm{H}} = 0. \quad (4.9)$$

This solution is valid provided $q \ll 1/M$, i.e. provided the cylinder is not nearly a perfect insulator. Note that the Hartmann balance breaks down near $\theta = \pm\frac{1}{2}\pi$ and the Coriolis terms need to be reinstated at that latitude for a full description of this mode. This singularity does not affect the large-scale structure or the drag, so it need not concern us further. This Hartmann solution is anomalous in that it is independent of both u_x and u_z; that is, motion in the direction of the cylinder axis or the applied magnetic field does not excite the Hartmann mode to dominant order. We shall see that this leads to difficulties in determining some components of drag.

Combining (2.11) and (4.9), we have that to dominant order

$$\frac{\boldsymbol{D}}{\sigma B^2 |U| a^2} = \pi(N_y^2 u_z - N_z^2 u_y)\,\hat{\boldsymbol{x}} + \pi(N_z^2 u_x - u_y - N_x^2 u_z)\,\hat{\boldsymbol{y}} - \frac{4u_z}{M}\,\hat{\boldsymbol{z}}. \tag{4.10}$$

Note that $\boldsymbol{D}$ is highly variable; the y-component is of order unity, but the others are much smaller.

It is anomalous that a drag term in the x-direction which is proportional to u_x does not occur in (4.10). This implies that motion of the cylinder in the direction of the applied magnetic field is a dissipationless process. However, such a motion must induce both electric currents and fluid motions, each of which dissipate energy. The desired drag term can arise only through the integral involving viscous terms in (2.11). This integral should produce the desired drag term if the part of ψ which is proportional to u_x has the same symmetry as $\sin(\theta)$, i.e., even in x and odd in y. This symmetry is expected of ψ, but unexpectedly, ψ_{H}, given by (4.9), is independent of u_x, so that no contribution arises from the Hartmann mode. Also, no contributions to (4.10) can come from the BH mode; it behaves linearly in the coordinates in the vicinity of $r = 1$, so that the second and third radial derivatives of ψ_{BH} are identically zero.

It is apparent that the desired drag term cannot arise from (2.11) or from the more precise version which does not make the usual boundary-layer approximation. This drag must come from the terms of order R_0 or R_m which were neglected in the governing equations at the outset. The derivation of this drag term is beyond the scope of the present paper.

Even though we are in the limit of high magnetic-field strength, only motion across the lines of force is subject to the hydromagnetic drag. Motions parallel to the field or parallel to the axis of the cylinder are subject to a much weaker drag.

5. Solution for weak rotation: $1/M \ll N_y \ll 1$ and $N_x^2 \ll N_y$

As in the previous case, the short-range balance yields a Hartmann layer; the Coriolis force does not affect this structure. However, this force does play an important role in the long-range Ruan structure, taking the place of the viscous force in balancing the Lorentz force. The equations governing the Ruan modes, abstracted from (2.2)–(2.4) by neglecting the viscous terms and the x-derivatives in the Coriolis terms and Laplacians, are

$$-N_y^2 \frac{\partial \psi}{\partial y} = \frac{\partial c}{\partial x}, \quad 0 = \frac{\partial w}{\partial x} + \frac{\partial^2 c}{\partial y^2}, \quad -N_y^2 \frac{\partial w}{\partial y} = \frac{\partial^2 \psi}{\partial x^2}. \tag{5.1}$$

Note that, unlike the case of very weak rotation, the Ruan modes involve the interaction of ψ with w and c.

The forcing for the flow is in the conditions on ψ, $\partial\psi/\partial r$ and w in (2.10). In the case $N_y \ll 1/M$ considered in §4, the forcing on ψ and w is accommodated by the BH mode, with the magnitudes of ψ and w in the Hartmann modes being smaller order. This ordering prevails as $N_y \to 1/M$. Consequently, we anticipate that in the present case,

the forcing on ψ and w is accommodated by the Ruan mode, with the magnitudes of ψ and w in the Hartmann modes again being of smaller order. This observation allows us to take advantage of symmetry in constructing the solutions for the Ruan modes. Specifically, the solutions driven by u_x or u_z have ψ even in x and odd in y, c odd in x and even in y, and w even in both variables. The solutions driven by u_y have ψ odd in x and even in y, c even in x and odd in y, and w odd in both variables.

As in the previous section, the long-range Ruan modes may be solved by Fourier transform in y. The solutions which possess the required symmetries and decay as $|x| \to \infty$, may be expressed as

$$\psi_{\mathrm{R}} = -\operatorname{sgn}(x)\, u_z \int_0^\infty \frac{\bar{w}(k)}{k} \sin(ky) \sin(\hat{x}) \exp(-|\hat{x}|)\, \mathrm{d}k$$
$$+ \int_0^\infty [u_x \bar{\psi}_x(k) \sin(ky) + \operatorname{sgn}(x)\, u_y \bar{\psi}_y(k) \cos(ky)] \cos(\hat{x}) \exp(-|\hat{x}|)\, \mathrm{d}k, \quad (5.2)$$

$$w_{\mathrm{R}} = u_z \int_0^\infty \bar{w}(k) \cos(ky) \cos(\hat{x}) \exp(-|\hat{x}|)\, \mathrm{d}k$$
$$- \int_0^\infty [u_y \bar{\psi}_y(k) \sin(ky) - \operatorname{sgn}(x)\, u_x \bar{\psi}_x(k) \cos(ky)] \sin(\hat{x}) \exp(-|\hat{x}|)\, k\, \mathrm{d}k, \quad (5.3)$$

$$c_{\mathrm{R}} = -\frac{N_y u_z}{\sqrt{2}} \int_0^\infty \frac{\bar{w}(k)}{k} \cos(ky) [\sin(\hat{x}) + \operatorname{sgn}(x) \cos(\hat{x})] \exp(-|\hat{x}|)\, \mathrm{d}k$$
$$- \frac{N_y}{\sqrt{2}} \int_0^\infty [u_y \bar{\psi}_y(k) \sin(ky) - \operatorname{sgn}(x)\, u_x \bar{\psi}_x(k) \cos(ky)]$$
$$\times [\cos(\hat{x}) - \operatorname{sgn}(x) \sin(\hat{x})] \exp(-|\hat{x}|)\, \mathrm{d}k, \quad (5.4)$$

where $\hat{x} = N_y k x/\sqrt{2}$.

The non-homogeneous conditions on ψ and w at $x^2 + y^2 = 1$ are satisfied provided $\bar{\psi}_x(k)$, $\bar{\psi}_y(k)$ and $\bar{w}(k)$ obey (4.4)–(4.6). As in §4, symmetry again requires that (4.7) be satisfied. The solutions for $\bar{\psi}_x(k)$, $\bar{\psi}_y(k)$ and $\bar{w}(k)$ are again given by (4.8). The dominant Hartmann modes are again given by (4.9).

Combining (2.11) and the solutions described above, we have

$$\frac{\boldsymbol{D}}{\sigma B^2 |U| a^2} = \pi(N_y^2 u_z - N_z^2 u_y)\, \hat{\boldsymbol{x}} + \pi(N_z^2 u_x - u_y - N_x^2 u_z)\, \hat{\boldsymbol{y}} - \frac{\pi N_y}{\sqrt{2}}(u_x + u_z)\, \hat{\boldsymbol{z}}. \quad (5.5)$$

Note the similarity to (4.10). As in §4, the drag in the x-direction driven by the flow in that direction is small, and is expected to come from the terms of order R_0 or R_m in the governing equations.

6. Solution for strong rotation: $1 \ll N$

In this parameter range the long-range structure is elongated in the direction of the rotation vector, rather than in the direction of the applied magnetic field. Consequently the drag is best expressed in the (ξ, η, z)-coordinate system (see figure 3). In this system the drag force expressed by (2.11) may be written as

$$\frac{\boldsymbol{D}}{\sigma B^2 |U| a^2} = \pi N^2 u_z \hat{\boldsymbol{\xi}} + \pi N_z^2 (u_\xi \hat{\boldsymbol{\eta}} - u_\eta \hat{\boldsymbol{\xi}}) + \int_{-\pi}^{\pi} \hat{\boldsymbol{z}} \cos(\omega - \gamma)(c)_{r=1}\, \mathrm{d}\omega$$
$$+ \frac{1}{M^2} \int_{-\pi}^{\pi} \left[\hat{\boldsymbol{y}} \left(\frac{\partial^3 \psi}{\partial r^3} \right)_{r=1} + \hat{\boldsymbol{\omega}} \left(\frac{\partial^3 \psi}{\partial r^3} - \frac{\partial^2 \psi}{\partial r^2} \right)_{r=1} + \hat{\boldsymbol{z}} \left(\frac{\partial w}{\partial r} \right)_{r=1} \right] \mathrm{d}\omega, \quad (6.1)$$

where $\hat{\boldsymbol{\omega}} = \cos(\omega)\hat{\boldsymbol{\eta}} - \sin(\omega)\hat{\boldsymbol{\xi}}$, $u_\xi = \cos(\gamma)u_x - \sin(\gamma)u_y$, $u_\eta = \sin(\gamma)u_x + \cos(\gamma)u_y$, and ω is the polar angle measured from the ξ-axis; $\theta = \omega - \gamma$ (see figure 3).

It appears that the dominant contribution to the drag force comes from the terms proportional to N^2 and N_z^2 in (6.1). However, these are 'lift' terms in which the resulting force is in a direction normal to the applied velocity. Further, most of the viscous terms in (6.1) are also of order N^2, and shall be retained. All terms of unit order are in fact small and may be neglected; in particular, the Lorentz drag is small. Keeping only the dominant terms, (6.1) may be simplified to

$$\frac{\boldsymbol{D}}{\sigma B^2 |U| a^2} = \pi N^2 u_z \hat{\boldsymbol{\xi}} + \pi N_z^2 (u_\xi \hat{\boldsymbol{\eta}} - u_\eta \hat{\boldsymbol{\xi}}) + \int_{-\pi}^{\pi} \left[\frac{(\hat{\boldsymbol{y}} + \hat{\boldsymbol{\omega}})}{M^2} \left(\frac{\partial^3 \psi}{\partial r^3} \right)_{r=1} + \frac{\hat{\boldsymbol{z}}}{M^2} \left(\frac{\partial w}{\partial r} \right)_{r=1} \right] \mathrm{d}\omega. \tag{6.2}$$

To calculate the drag from (6.2) we need only the Ekman-layer solutions. However, they depend on the structure of the large-scale mode, which needs to be calculated first. In the large-scale structure the primary balance is still between Coriolis and Lorentz forces. The equations governing the new structure may be abstracted from (2.2)–(2.4), rewritten using (3.2) and (3.3), by ignoring viscous terms and neglecting η-derivatives compared with ξ-derivatives. They are

$$-N^2 \frac{\partial \psi}{\partial \eta} = \cos(\gamma) \frac{\partial c}{\partial \xi}, \quad 0 = \cos(\gamma) \frac{\partial w}{\partial \xi} + \frac{\partial^2 c}{\partial \xi^2}, \quad -N^2 \frac{\partial w}{\partial \eta} = \cos^2(\gamma) \frac{\partial^2 \psi}{\partial \xi^2}. \tag{6.3}$$

These equations yield one mode; they are capable of satisfying only one boundary condition, on either ψ or w. The Ekman-layer structure has two modes and will satisfy the remaining two velocity conditions. The fourth exterior mode is governed by the Laplacian of c. It can be shown by scaling arguments that the new mode must satisfy the non-homogeneous boundary condition on ψ, while the Ekman modes satisfy those on $\partial\psi/\partial r$ and w. The condition on ψ from (2.10) may be expressed as

$$\psi = u_\xi \sin(\omega) - u_\eta \cos(\omega) = u_\xi \operatorname{sgn}(\eta)(1-\xi^2)^{\frac{1}{2}} - u_\eta \xi. \tag{6.4}$$

As in the previous sections, this non-homogeneous condition on ψ dictates the pattern of symmetry in the solution. The solution driven by u_ξ has ψ even in ξ and odd in η, c odd in ξ and even in η, and w even in both variables, while that driven by u_η has ψ odd in ξ and even in η, c even in ξ and odd in η, and w odd in both variables.

The large-scale structure may be treated in a manner similar to that of the BH and Ruan structures in the previous sections. Contraction of the η-axis by a factor $N^2/\cos^2(\gamma)$ collapses the cylinder to the ξ-axis and the equation for ψ becomes the Laplacian, which can be solved by Fourier transform in ξ. The solution of (6.3) may be expressed as

$$\psi_{\mathrm{N}} = \int_0^\infty [u_\xi \operatorname{sgn}(\eta) \bar{\psi}_\xi(k) \cos(k\xi) + u_\eta \bar{\psi}_\eta(k) \sin(k\xi)] \exp(-k|\lambda|)\, \mathrm{d}k, \tag{6.5}$$

$$w_{\mathrm{N}} = \int_0^\infty [-u_\xi \bar{\psi}_x(k) \cos(k\xi) - u_\eta \operatorname{sgn}(\eta) \bar{\psi}_\eta(k) \sin(k\xi)] k \exp(-k|\lambda|)\, \mathrm{d}k \tag{6.6}$$

and

$$c_{\mathrm{N}} = \cos(\gamma) \int_0^\infty [-u_\eta \operatorname{sgn}(\eta) \bar{\psi}_\eta(k) \cos(k\xi) + u_\xi \bar{\psi}_\xi(k) \sin(k\xi)] \exp(-k|\lambda|)\, \mathrm{d}k, \tag{6.7}$$

where $\eta = \lambda N^2/\cos^2(\gamma)$. The subscript N denotes this new mode.

This mode satisfies the boundary condition (6.4) on ψ in the interval $|\xi| < 1$, i.e.

$$\int_0^\infty \bar{\psi}_\xi(k)\cos(k\xi)\,dk = (1-\xi^2)^{\frac{1}{2}} \tag{6.8}$$

and

$$\int_0^\infty \bar{\psi}_\eta(k)\sin(k\xi)\,dk = -\xi \tag{6.9}$$

plus the symmetry condition for $1 < |\xi|$:

$$\int_0^\infty \bar{\psi}_\xi(k)\cos(k\xi)\,dk = 0. \tag{6.10}$$

As in §5, we have that

$$\bar{\psi}_\xi(k) = J_1(k)/k \quad \text{and} \quad \bar{\psi}_\eta(k) = -J_1(k)/k. \tag{6.11}$$

The short-range balance reduces to an Ekman balance to dominant order; the Lorentz force does not affect this structure. The equations governing the Ekman modes, abstracted from (2.2) and (2.4) are

$$-M^2N^2\sin(\omega)\,\psi = \frac{\partial w}{\partial r} \quad \text{and} \quad M^2N^2\sin(\omega)\,w = \frac{\partial^3\psi}{\partial r^3}. \tag{6.12}$$

The Ekman modes are driven by the conditions on $\partial\psi/\partial r$ and w, from (2.10), with contributions from solution (6.10) and (6.11). The solutions of equations (6.18)–(6.19) are

$$w_E = \exp(-\bar{r})[w_c(\omega)\cos(\bar{r}) + w_s(\omega)\sin(\bar{r})], \tag{6.13}$$

$$\psi_E = \frac{\operatorname{sgn}(\omega)\,E^{\frac{1}{2}}}{\sqrt{2}|\sin(\omega)|^{\frac{1}{2}}}\exp(-\bar{r})\{[w_c(\omega)-w_s(\omega)]\cos(\bar{r}) + [w_s(\omega)+w_c(\omega)]\sin(\bar{r})\}, \tag{6.14}$$

where

$$w_c = u_\xi - u_\eta\cot(\omega) + u_z, \quad w_s = u_\xi/|\sin(\omega)| \tag{6.15}$$

and $\bar{r} = (|\sin(\omega)|/2E)^{\frac{1}{2}}(r-1)$.

With these solutions, we may evaluate the integrals appearing in (6.2) and write

$$\frac{\boldsymbol{D}}{\sigma B^2|\boldsymbol{U}|a^2} = -\pi(N^2u_\xi + N_z^2u_\eta)\,\hat{\boldsymbol{\xi}} + \pi(N_z^2u_\xi - N^2u_\eta)\,\hat{\boldsymbol{\eta}} + \frac{N}{M}(4.0275u_\xi - 3.3889u_z)\,\hat{\boldsymbol{z}}. \tag{6.16}$$

The drag is highly anisotropic with the largest diagonal term, of order N^2, being that in the ξ-direction, i.e. the direction perpendicular to the plane of the cylinder axis and the rotation axis. There is an associated lift of order N^2 in the η-direction, i.e. perpendicular to the axis of the cylinder, in the plane of the rotation axis. The diagonal term in the η-direction is of unit order, while that in the z-direction, i.e. along the axis of the cylinder is smallest.

7. Summary and discussion

The flow structures generated by the prescribed motion of a rigid cylinder through a rotating electrically conducting fluid in the presence of an applied magnetic field have been identified. In the case that the Lorentz force is larger than the Coriolis force, the dominant flow structure is large scale, elongated in the direction of the applied magnetic field. This elongation serves to weaken the Lorentz force sufficiently that

a balance can be achieved. In the case of very weak rotation ($\Omega_y < \nu/a^2$ and $\Omega_x < (\sigma\nu)^{\frac{1}{2}} B/\rho^{\frac{1}{2}}a$), this balance is between Lorentz and viscous forces, and the necessary elongation is large, of order the Hartmann number, M, time the cylinder radius. In the case of weak rotation ($\nu/a^2 < \Omega_y < \sigma B^2/\rho$ and $\Omega_y < \rho\Omega_x^2/\sigma B$), the balance is magnetostrophic (between Lorentz and Coriolis) and the necessary elongation is less extreme, of order $N_y = (2\rho\,\Omega_y/\sigma B^2)^{\frac{1}{2}}$ times the cylinder radius.

The situation is reversed for the case of strong rotation ($\sigma B^2/\rho < \Omega_\perp$ where $\Omega_\perp$ is the magnitude of the rotation vector perpendicular to the axis of the cylinder); now the large-scale structure is elongated in the direction of the rotation axis, weakening the Coriolis force so that the Lorentz force is able to balance it. This structure is similar to the classic Taylor column (e.g. see Moore & Saffman 1969), but is significantly shorter, as the Lorentz force is stronger than the viscous force in the limit of large Hartmann number; the elongation is of order $N^2 = 2\rho\Omega_\perp/\sigma B^2$ times the cylinder radius.

The drag expressions (4.10), (5.5) and (6.16) may be summarized by writing

$$\boldsymbol{D} = \sigma B^2 a^2 \boldsymbol{T}_{ij}\, U_j\, \hat{\boldsymbol{x}}_i \tag{7.1}$$

where

$$U^T = [U \quad V \quad W] \tag{7.2}$$

is the velocity vector, $\hat{\boldsymbol{x}}_1 = \hat{\boldsymbol{x}}$, $\hat{\boldsymbol{x}}_2 = \hat{\boldsymbol{y}}$, $\hat{\boldsymbol{x}}_3 = \hat{\boldsymbol{z}}$ and $\boldsymbol{T}$ is the tensor of drag coefficients.

For very weak rotation ($N_y \ll 1/M$ and $N_x \ll 1/M^{\frac{1}{2}}$)

$$\boldsymbol{T} = \begin{bmatrix} 0 & -\pi N_z^2 & \pi N_y^2 \\ \pi N_z^2 & -\pi & -\pi N_x^2 \\ 0 & 0 & -\dfrac{4}{M} \end{bmatrix}. \tag{7.3}$$

For weak rotation ($1/M \ll N_y \ll 1$ and $N_x^2 \ll N_y$)

$$\boldsymbol{T} = \begin{bmatrix} 0 & -\pi N_z^2 & \pi N_y^2 \\ \pi N_z^2 & -\pi & -\pi N_x^2 \\ 0 & 0 & -\dfrac{4N_y}{\sqrt{2}} \end{bmatrix}. \tag{7.4}$$

For strong rotation ($1 \ll N$)

$$\boldsymbol{T} = \begin{bmatrix} -\pi N^2 & -\pi N_z^2 & 0 \\ \pi N_z^2 & -\pi N^2 & 0 \\ 4.0275\dfrac{N}{M} & 0 & -3.3889\dfrac{N}{M} \end{bmatrix}. \tag{7.5}$$

We expect that the diagonal components of the drag tensors will have negative coefficients. (More precisely, the tensors should have eigenvalues with negative real parts; they do so.) Of the nine diagonal coefficients in (7.3)–(7.5), seven are negative, but two are zero. The solutions given in (7.3)–(7.5) represent the leading-order terms in a double Taylor expansion in powers of Rossby number and magnetic Reynolds number. It happens that two of the drag coefficients are zero to this leading order, and it is anticipated that these coefficients will be found to be negative at the next order in the expansion.

In the cases of very weak rotation and of weak rotation, the largest entry in the drag tensor is that resisting motion across magnetic field lines. The next largest entry is that

resisting motion of the cylinder parallel to its axis. To this order, there is no resistance to motion parallel to magnetic field lines. The lift forces induced by the Coriolis force are smaller than the non-zero resistive components.

In the case of strong rotation, the situation is somewhat different. The resistive and lift components in the plane normal to the cylinder axis are all of comparable magnitude and large, while those involving the direction parallel to the cylinder axis are smaller. In all three cases considered, the resistance to motion of the cylinder parallel to its axis is of smaller order than resistance to transverse motion. Consequently, the motion in response to a specified forcing is in general not aligned with the direction of that forcing.

Consider for example a cylinder rising freely under the action of a buoyancy force produced by a density deficit, $\Delta\rho = \rho_c - \rho$, where ρ_c is the density of the cylinder. The buoyancy force per unit length acting on the cylinder is given by (3.5) of Ruan & Loper (1993). In equilibrium, the sum of the buoyancy force and the drag is zero. This condition may be solved for the velocity in terms of the orientation of gravity:

$$U_j = -\frac{(\Delta\rho)\pi}{\sigma B^2} T_{ij}^{-1} g_i. \tag{7.6}$$

This gives the speed and direction of rise of the cylinder in relation to the magnitude and orientation of the buoyancy force. Note that expression (7.6) does not contain the radius of the buoyant cylinder as an explicit parameter. Further the radius appears in the definition of M, but not of N. It follows that the rise speed is relatively insensitive to the size of the cylinder.

The author wishes to acknowledge the advice and encouragement provided by H. K. Moffatt, and to thank the National Science Foundation, Earth Sciences Division, for support of this research under grant EAR-9116956, and the North Atlantic Treaty Organization for Collaborative Research Grant 910117, which made possible the interaction with H. K. Moffatt. This is contribution #349 of the Geophysical Fluid Dynamics Institute, Florida State University.

REFERENCES

BRAGINSKY, S. I. 1960 Magnetohydrodynamics of weakly conducting liquids. *Sov. Phys. JETP* **37**, 1005–1014.

BRAGINSKY, S. I. 1963 Structure of the F layer and reasons for the convection in the Earth's core. *Sov. Phys. Dokl.* **149**, 8–10.

CHEN, C. F. & CHEN, F. 1991 Experimental study of directional solidification of aqueous ammonium chloride solution. *J. Fluid Mech.* **227**, 567–586.

ELTAYEB, I. A. & LOPER, D. E. 1991 On the stability of vertically oriented double-diffusive interfaces. Part 1: A single plane interface. *J. Fluid Mech.* **228**, 149–181.

GRADSHTEYN, I. S. & RYZHIK, I. M. 1980 *Tables of Integrals, Series and Products*. Academic.

HASIMOTO, H. 1960 Steady longitudinal motion of a cylinder in a conducting fluid. *J. Fluid Mech.* **8**, 61–81.

LOPER, D. E. & MOFFATT, H. K. 1993 Small-scale hydromagnetic flow in the Earth's core: rise of a vertical buoyant plume. *Geophys. Astrophys. Fluid Dyn.* **68**, 177–202.

LOWES, F. J. 1984 The geomagnetic dynamo–elementary energetics and thermodynamics. *Geophys. Surv.* **7**, 91–107.

MOFFATT, H. K. & LOPER, D. E. 1993 The magnetostrophic rise of a buoyant parcel in the Earth's core. *Geophys. J. Intl* (to appear).

MOORE, D. W. & SAFFMAN, P. G. 1969 The structure of free vertical shear layers in a rotating fluid and the motion produced by a slowly rising body. *Phil. Trans. R. Soc. Lond.* A **264**, 597–634.

RUAN, K. 1993 On the motion of a rigid cylinder parallel to its axis in a rotating electrically conducting fluid. PhD dissertation, Florida State University.

RUAN, K. & LOPER, D. E. 1993 On small-scale hydromagnetic flow in the Earth's core: Motion of a rigid cylinder parallel to its axis. *J. Geomag. Geoelec.* (to appear).

TAIT, S. & JAUPART, C. 1989 Compositional convection in viscous melts. *Nature* **338**, 571–574.

TAIT, S. & JAUPART, C. 1992 Compositional convection in a reactive crystalline mush and melt differentiation. *J. Geophys. Res.* **97**, 6735–6756.